

Detection of DNA by Graphene-on-Silicon FET Structures Simultaneously at DC and 101 GHz

E.R. Brown and W-D. Zhang

Department of Physics and Electrical Engineering, Wright State University, Dayton, OH 45435 USA

D. Neff, N.S. Green, and M.L. Norton

Department of Chemistry, Marshall University
Huntington, WV, USA

P.H.Q. Pham and P.J. Burke

Department of Electrical and Computer Engineering
University of California, Irvine, CA, USA

Abstract— Two graphene-silicon field-effect transistor samples are characterized as a biological sensor of single-stranded DNA at DC and 101 GHz. In the first sample the 13-mer DNA is detected at DC and 101 GHz at three different molarities: 0.01, 1.0 and 100 nM. In the second sample it is so detected at only 1.0 nM but under progressive dilution by de-ionized water. In both cases, the mechanism for detection appears to be the same: (1) at DC it is the DNA-induced decrease in sheet conductance, and (2) at 101 GHz it is a correlated decrease in RF sheet conductance and the associated increase in 101-GHz transmission through the GFET acting as an optical etalon.

Keywords—graphene, sheet conductance, DNA, silicon etalon, millimeter waves, graphene field effect transistor, backgate.

I. INTRODUCTION

While not the panacea for electronics that some predicted just a decade ago, graphene continues to attract interest for its wide array of applications such as sensing of biomolecular nucleic acids and proteins [1]. Two drivers for biosensing are the extreme sensitivity that monolayer graphene naturally has toward surface conditions, and the strong sp^2 -hybridized bonding behavior that graphene displays [2,3]. However, the sp^2 bonding is sensitive to the primary molecular structure, but not so much to the higher-order structure [4]. So a possible method of discriminating macromolecules is through their π - π stacking [5] and high-frequency dielectric behavior [6,7]. It is known that there is unique dielectric dispersion and low-lying vibrational resonance in macromolecules, especially the nucleic acids [8]. Here we support the longstanding proposal that biosensor detection and selectivity may ultimately be practical through these unique signatures, especially at GHz-to-THz frequencies [9,10]. However, we also show that the experimental behavior can be complex in ways that are not yet fully understood.

II. EXPERIMENTAL METHOD

A cross-sectional view of the graphene-silicon field-effect transistor (GFET) structure is shown in Fig. 1(a), and the fabrication method is described in Ref. [11]. The graphene is deposited on a high-resistivity Si substrate with thin oxide layer inbetween. The source (S) and drain (D) contacts are deposited directly on the graphene, and a (back) contact (G) on the opposite side of the Si to create gating action. Although having low transconductance by Si-MOS standards, this GFET is quite

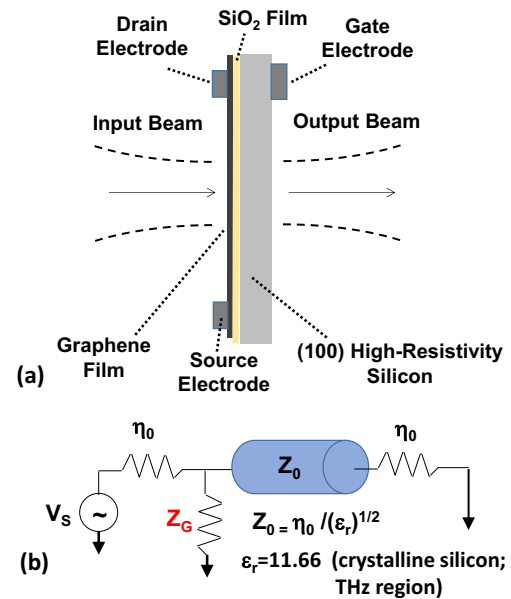


Fig. 1. (a) GFET configuration with respect to 101-GHz beam. (b) Equivalent-circuit model.

useful for studying the transport physics of graphene, especially in comparing the high-frequency (THz) to the DC behavior [12]. More recently, we applied the same structure to detect the presence of single-stranded DNA [13]. A similar graphene film has already been demonstrated for chemical detection but on a PDMS substrate rather than Si [14].

The GFET is used for biomolecular sensing by exposing the graphene film to solution and measuring changes in its DC and RF sheet conductance. The effect of the biomolecules on the RF sheet conductance is estimated via the transmittance T of radiation propagating perpendicular to the graphene, as shown in Fig. 1(a). Assuming focused Gaussian-beam propagation, we can treat the radiation as quasi-plane waves and model T with the transmission line model in Fig. 1(b), in which graphene is simply a shunt, lumped impedance Z_G . The length of the transmission line L is equal to the thickness of the high-resistivity silicon substrate, and its characteristic impedance η_0 is equal to $\eta_0/n = 110 \Omega$, where $n = (\epsilon_r)^{1/2} = 3.415$ and $\epsilon_r = 11.66$: the relative dielectric constant of the Si in the 100-1000 GHz range [15]. Circuit analysis then predicts T as the ratio between the power delivered to the free space load (lumped element η_0) and the available power from the source on the incident side.

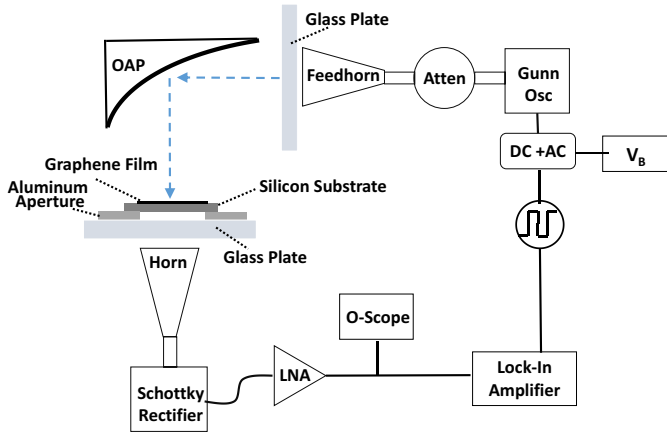


Fig. 2. Experimental set-up for 101-GHz GFET transmittance.

Fig. 2 shows the 101-GHz experimental set-up which consists of a waveguide-mounted (WR-10) Gunn-oscillator as the source, and a WR-10-mounted Schottky rectifier as the receiver. The Gunn oscillator is square-wave amplitude modulated with a power-MOSFET circuit, and coupled to free space through a pyramidal horn antenna. This feeds an off-axis paraboloid which directs and focuses the beam downward. The focused beam is mode-matched to a second feedhorn that collects the radiation into the Schottky receiver. Glass plates 0.5-inch-thick are located close to the mouth of both feedhorns to act as ~ 7 dB spatial attenuators and reduce standing wave effects. The GFET structure is located in the beam path above the receive attenuator where the spot size is approximately 5 mm. The output signal from the Schottky rectifier is fed to a 1000x-gain low-noise voltage amplifier, and then demodulated with a lock-in amplifier synchronized to the square wave. A waveguide attenuator between the Gunn oscillator and the feedhorn allows the received signal to be increased to the maximum possible output signal-to-noise ratio (SNR) before the onset of compression and other nonlinearity. Typically, this background SNR was ~ 60 dB.

III. DESIGN AND VALIDATION

Fig. 3(a) shows the predicted T through the GFET as a function of frequency and parameterized by the graphene sheet impedance assuming the imaginary part is negligible, so that $Z_G \approx (G_G)^{-1}$. Our previous results showed that this approximation is quite valid at ~ 100 GHz but becomes less accurate with increasing frequency [12]. The range of parametrized sheet conductance G_G is 0.5 to 19.2 mS, corresponding to $8 \cdot G_0$ to $316 \cdot G_0$, where $G_0 = \pi e^2 / 2h$ is the fundamental optical (interband) conductance in graphene [16]. The graphene tested in this work typically displays DC conductance between 0.3 and 2.2 mS (≈ 5 to $35 \cdot G_0$) consistent with the intraband conductivity being much higher than the interband in single-layer graphene. For each G in Fig. 3, T displays the oscillatory behavior characteristic of all parallel-plate (e.g., Fabry-Perot) etalons with peak-to-peak separation $\Delta f = c/2nL = 112$ GHz for $L = 392$ μm . The peaks do not quite reach unity transmission since the etalon is optically unbalanced.

Very important for our bio-detection experiments is the sensitivity factor, estimated as the first derivative of T with respect to the graphene conductance at a fixed frequency:

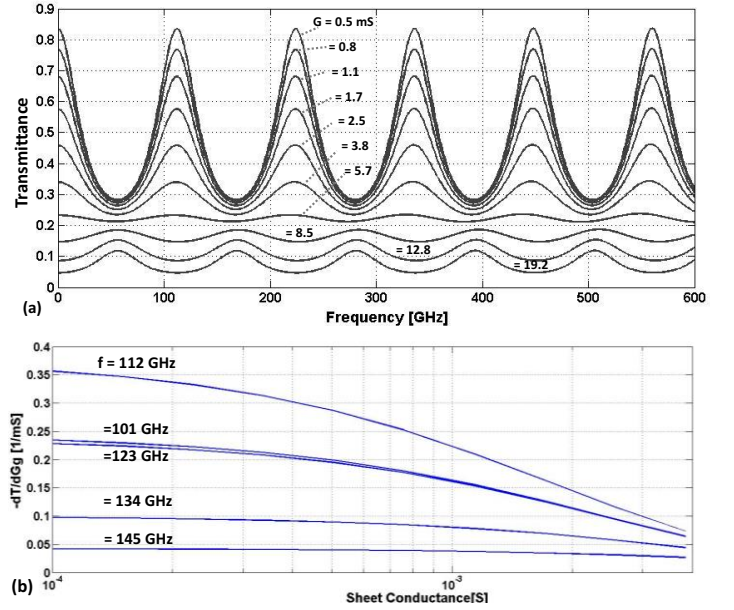


Fig. 3. (a) Transmittance of GFET vs frequency parameterized by graphene sheet conductance. (b) Sensitivity factor vs graphene sheet conductance parameterized by frequency.

$\partial T / \partial G_G|_f$. From Fig. 3(a) we expect it to be much greater near the peaks of T than near the valleys. This is justified graphically in Fig. 3(b) where we plot the theoretical $\partial T / \partial G_G|_f$ vs G_G around the fundamental-resonance peak in 2(a) centered at 112 GHz. For $G_G = 1.0$ mS - a typical value for our GFETs - we see that $\partial T / \partial G_G|_f$ decreases by $\approx 5x$ between 112 and 145 GHz, but only by $\approx 40\%$ between 112 and our operational frequency of 101 GHz.

The GFET samples were operated with the backgate bias from a low-noise power supply, and a drain-source constant-voltage bias of $V_{DS} = +0.1$ V from a Keithley 2400 source meter. This backgate voltage V_G was chosen as a compromise. The smaller the V_G , the higher the G_G and the lower the sensitivity factor according to Fig. 3(b). On the other hand, operation near the Dirac point (where G_G approaches zero) was found to cause large drain-source current fluctuation. So the V_G in each device was set somewhat below the Dirac voltage. And because the graphene geometry between the S and D electrodes is approximately square (area ≈ 1 cm^2), the absolute DC sheet conductance was recorded as $G_{DC} \approx I_{DS} / V_{DS}$. For example, sample#1 had a Dirac voltage of ≈ 30 V and was biased with $V_G = 25$ V where I_{DS} was 0.2132 mA at $V_{DS} = 0.1$, so $G_G = 2.13$ mS. For sample#2 the Dirac voltage was ≈ 25 V and the backgate voltage was set at 20 V where I_{DS} was 0.0383 mA at $V_{DS} = 0.1$ V, so $G_G = 0.383$ mS.

To validate the measurement technique and assess its accuracy, we used the backgate to induce a known-change in graphene DC sheet conductance and compare this with the change of the 101-GHz sheet conductance, knowing from our previous results [12] that the two should be nearly equal. For sample #1 we applied backgate voltages of $V_{HI} = 30$ V and $V_{LO} = 20$ V to straddle the nominal +25 V and allow for mean-value estimation. The DC current values at the two gated voltages were 0.2017 and 0.2255 mA, respectively,

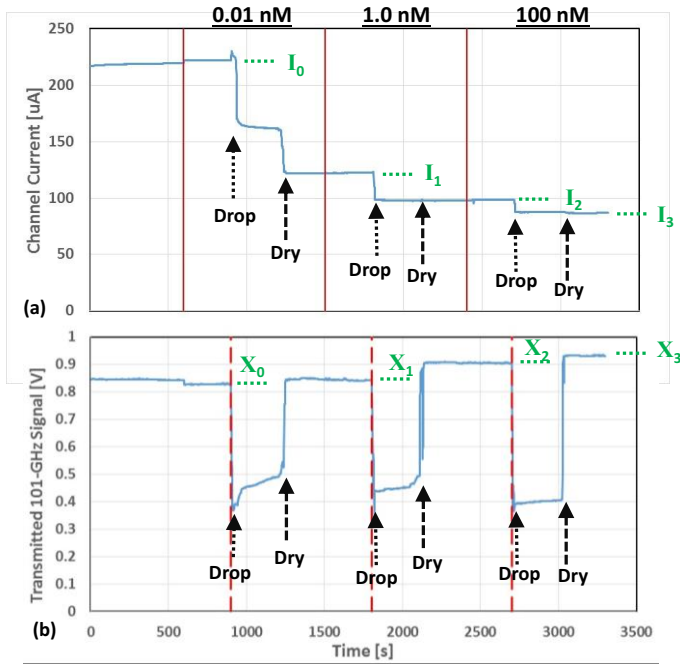


Fig. 4. Sample#1 current (a) and transmitted 101-GHz signal (b) vs time.

corresponding to $\Delta G_{DC} = \Delta I / 0.1 = -0.238$ mS. The 101-GHz lock-in signals for the same backgate voltages were $X_{HI} = 0.8661$ and $X_{LO} = 0.8412$, and the background signal (no GFET) was $X_B = 0.8527$ V, where all four significant digits are relevant given the good signal-to-noise ratio. These yield to a transmittance difference of $\Delta T \equiv T_{HI} - T_{LO} \approx (X_{HI} - X_{LO}) / X_B = 0.0292$. From Fig. 3(b) the sensitivity factor at $G_G = 2.13$ mS is $\partial T / \partial G_G \approx -0.11$ mS⁻¹. Hence the derived change of RF sheet conductance is $\Delta G_{rf} = \Delta T / (\partial T / \partial G_G) \approx -0.265$ mS in acceptable agreement with ΔG_{DC} .

IV. EXPERIMENT RESULTS: SAMPLE#1

The biodetection protocol for sample#1 was to apply 13-mer single-stranded DNA solutions of three different molarities (0.01 nM, 1.0 nM, and 100 nM) sequential at 900-s intervals, starting with the 0.01 nM solution. A droplet of each was placed directly on the graphene with a syringe, allowed to settle for 300 s, and then blown dry with an oil-free air gun. The Keithley-2400 DC current was recorded simultaneous with the 101-GHz transmitted signal via the output from the lock-in amplifier. The experimental results for DC current are shown in Figs. 4(a) where we see an initial value of 222 uA between ≈ 600 and 900 s, corresponding to an initial sheet conductance of 2.22 mS. Then a large fall in DC current occurs with the application of all three droplets, and a lesser fall upon blow drying 300 s later. Both effects are most pronounced with the 0.01 nM solution and become progressively weaker with the other two. The 1.0 and 100 nM droplets have a significant effect in their aqueous form but little further change occurs upon drying. *In all cases, however, by decreasing the current at constant voltage, the DNA is decreasing the DC sheet conductance of the graphene.*

Similarly, the transmitted THz signal plotted in Fig. 4(b) shows a large and precipitous decrease upon application of

each droplet of DNA solution. But unlike the DC current, the THz signal recovers to its previous level and goes slightly higher upon drying. The strong decrease and recovery can be explained by the absorption coefficient of ~ 100 cm⁻¹ for liquid water at 101-GHz. Although each droplet is ~ 1 mm thick, it doesn't fill the entire beam footprint in Fig. 1 so the net attenuation caused by the liquid water is < 10 dB. From Fig. 3, the increased post-dry transmission level compared to initial level suggests that the 101-GHz sheet conductance, like the DC conductance, is decreasing with each droplet.

To quantify and compare the effects of the DNA on the DC and 101-GHz signals, we define and calculate relative sheet-conductance changes, ΔG_{dc} and ΔG_{rf} , and the normalized changes $\Delta G'_{dc}$ and $\Delta G'_{rf}$. The DC values are defined according to Fig. 4(a) as $\Delta G_{dc} \equiv (I_N - I_0) / 0.1$ V, where the I_N ($N = 1, 2,$ and 3) are the plateau average current levels after drying of the 0.01, 1.0, and 100 nM droplets, respectively. And the normalized value $\Delta G'_{dc} \equiv (I_N - I_0) / I_0 / 0.1$ V, where I_0 is the initial average value, 0.22 mA. The RF values are given by $\Delta G_{rf} \equiv (X_N - X_0) / (\partial T / \partial G_G)$ where the X_N ($N = 1, 2,$ and 3) are the plateau transmitted signals, and again $\partial T / \partial G_G \approx -0.11$ mS⁻¹. And the normalized quantity $\Delta G'_{rf} \equiv [(X_N - X_0) / X_0] / (\partial T / \partial G_G)$, where X_0 is the initial average transmitted signal, 0.828 V. As listed in Table I, ΔG_{dc} and ΔG_{rf} both increase in magnitude monotonically with molarity but with a sub-linear dependence such that ΔG_{dc} changes $< 40\%$ over the entire range. Interestingly, the ΔG_{rf} is always smaller in magnitude than ΔG_{dc} , especially for 0.01 nM where it is approximately 5-times lower. The reason for this is not yet understood.

V. EXPERIMENTAL RESULTS: SAMPLE#2

The biodetection protocol for sample#2 was to apply only 1.0-nM, 13-mer single-stranded DNA solution, and follow this up with successive applications of de-ionized (DI) water. This protocol was designed to test the reproducibility of the DNA-on-graphene effect, and also the possibility of reversing it by removal of the DNA. The experimental results for DC current

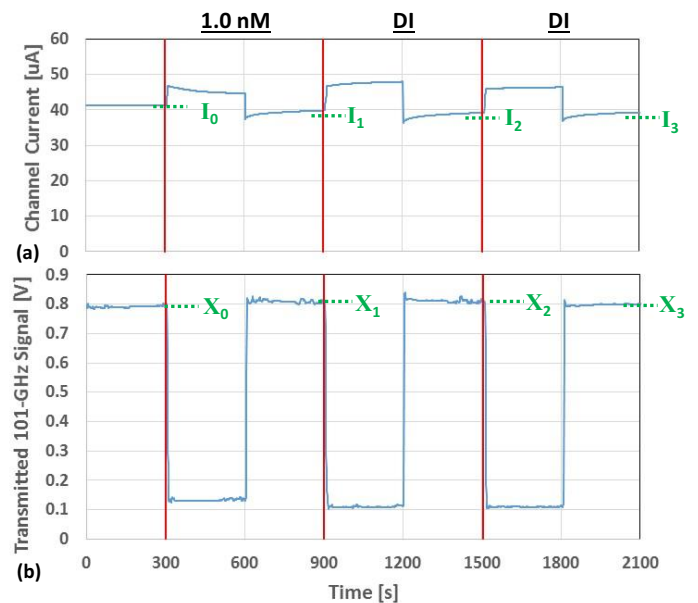


Fig. 5. Sample#2 current (a) and transmitted 101-GHz signal (b) vs time.

TABLE I. METRICS FOR TWO GFET SAMPLES

Sample#1				
Droplet	ΔG_{dc} [mS]	$\Delta G'_{dc}$ [1/V]	ΔG_{rf} [mS]	$\Delta G'_{rf}$ [mS]
0.01 nM DNA	-9.98E-01	-4.49E-01	-1.89E-01	-2.29E-01
1.0 nM DNA	-1.24E+00	-5.58E-01	-8.62E-01	-1.04E+00
100 nM DNA	-1.35E+00	-6.09E-01	-1.14E+00	-1.38E+00
Sample#2				
Droplet	ΔG_{dc} [mS]	$\Delta G'_{dc}$ [1/V]	ΔG_{rf} [mS]	$\Delta G'_{rf}$ [mS]
1.0 nM DNA	-8.49E-02	-2.06E-01	-1.93E-02	-2.43E-02
DI Water	-9.57E-02	-2.32E-01	-2.65E-02	-3.35E-02
DI Water	-3.37E-02	-8.18E-02	-2.42E-02	-3.06E-02

and 101-GHz transmitted signal are plotted in Figs. 5(a) and (b), respectively. The initial condition was dry and intended to show the stability of the measured quantities, and after 300 s the DNA droplet was applied. Similar to sample#1, the DNA droplet decreased the 101-GHz signal [Fig. 5(b)], but in contrast it increased the drain source current [Fig. 5(a)]. After letting the droplet sit for 300 s, the sample was blown dry, and the impact on the DC current and 101-GHz signal was then the same qualitatively as for sample#1; i.e., the DC current *decreased* to a level below the starting value, and the 101-GHz transmittance *increased*.

The protocol was completed by application of 2 DI water droplets successively at 900 and 1500 s, and drying 300 s after each. As shown in Fig. 5(a), the effect on the DC was almost identical to that of the initial DNA droplet: an initial increase in current followed by a decrease after drying. Also notice a significant drift in the current even after drying. The effect on 101-GHz was quite similar to that from the first DNA droplet but the level after each successive drying appears to be asymptotically approaching the initial level; i.e., *the effect of the DNA is being reversed*. Furthermore, it shows a smaller degree of RMS variation than the DC current, lacking in the drift. This yields a higher signal-to-noise ratio than the DC signal when measured over the 300-s duration.

As with sample #1, we quantify the changes by ΔG_{dc} , $\Delta G'_{dc}$, ΔG_{rf} , and $\Delta G'_{rf}$, as defined above in Sec. IV, except now I_N ($N=1, 2$, and 3) are the plateau average current levels after drying of the 1.0-nM droplet and two subsequent DI droplets, respectively, with $I_0 = 41.2 \mu\text{A}$. And the X_N ($N=1, 2$, and 3) in the definition of ΔG_{rf} , and $\Delta G'_{rf}$ are the corresponding plateau-average 101-GHz signals corresponding to I_N , with $X_0 = 0.791 \text{ V}$. According to Fig. 3(b), $\partial T/\partial G_G$ is now $\approx -0.21 \text{ mS}^{-1}$ (compared to -0.11 mS^{-1} for sample#1) because of the much lower sheet conductance (0.412 mS) of sample#2 compared to sample#1 (2.22 mS) at their respective bias voltages. The resulting values of ΔG_{dc} , $\Delta G'_{dc}$, ΔG_{rf} , and $\Delta G'_{rf}$ are listed in Table I. The fair comparison is between the normalized quantities for the 1.0-nM-DNA droplet conditions where we see $\Delta G'_{dc}$ for sample#1 is about 2.7x greater than that for sample#2, but $\Delta G'_{rf}$ is over 10x greater. This reflects a large variation in DNA detection sensitivity between samples.

VI. CONCLUSION

We have presented the first known detection of DNA by single-layer graphene simultaneously at DC and a millimeter-

wave frequency, 101 GHz. Although the DC detection is more sensitive, there is room for improvement in the mm-wave performance through optimization of the experimental parameters. The mm-wave detection opens up the exciting possibility of enhancing the selectivity of the GFET towards nucleic acids vs many other possible analytes by further characterization of the frequency-dependence and possible vibrational resonances that nucleic acids are known to display at GHz-to-THz frequencies.

ACKNOWLEDGMENT

This material is based upon work supported by, or in part by, the U.S. Army Research Laboratory and the U.S. Army Research Office under contract number W911NF-11-1-0024.

REFERENCES

- [1] N. S. Green and M. L. Norton, "Interactions of DNA with graphene and sensing applications of graphene field-effect transistor devices: A review," *Anal. Chim. Acta* **853**, pp. 127-142, 2015.
- [2] S. Manohar, A. R. Mantz, K. E. Bancroft, C. Y. Hui, A. Jagota, and D. V. Vezenov, "Peeling single-stranded DNA from graphite surface to determine oligonucleotide binding energy by force spectroscopy," *Nano Lett.* **8**, pp. 4365-4372, 2008.
- [3] X-C. Dong, Y-M. Shi, W. Huang, P. Chen, and L-J. Li, "Electrical detection of DNA hybridization with single-base specificity using transistors based on CVD-grown graphene sheets" *Advanced Materials* **22**, pp. 1649-1653, 2010.
- [4] C. T. Lin, P. T. Loan, T. Y. Chen, K. K. Liu, C. H. Chen, K. H. Wei, *et al.*, "Label-free electrical detection of DNA hybridization on graphene using Hall effect measurements: revisiting the sensing mechanism," *Adv. Func. Mater.* **23**, pp. 2301-2307, 2013.
- [5] E. Dubuisson, Z. Yang, and K-P. Loh, "Optimizing label-free DNA electrical detection on graphene platform," *Anal. Chem.* **83**, 2452-2460, 2011.
- [6] H. J. Lee and J. G. Yook, "Recent research trends of radio-frequency biosensors for biomolecular detection," *Biosens. Bioelectron.* **61**, pp. 448-459, 2014.
- [7] I. Iramnaaz, Y. Xing, K. Xue, Y. Zhuang, and R. Fitch, "Graphene based RF/microwave impedance sensing of DNA," *IEEE Elec. Compon. Tech. Conf.* **61**, pp. 1030-1034, 2011.
- [8] R. Holzel, "Dielectric and dielectrophoretic properties of DNA," *IET Nanobiotechnol.* **3**, Issue 2, 28-45, 2009.
- [9] A. Wittlin, L. Genzel, F. Kremer, D. Häselser, and A. Poglitsch, "Far-infrared spectroscopy on oriented films of dry and hydrated DNA," *Phys. Rev. A* **34**, 493-500, 1986.
- [10] T. R. Globus, *et al.*, "THz spectroscopy of biological molecules," *J. Bio. Phys.* **29**, 89-100, 2003.
- [11] N. Rouhi, S. Capdevila, D. Jain, K. Zand, Y-Y. Wang, E. R. Brown, L. Jofre, and P.J. Burke "THz graphene optics", *Nano Research*, Online FirstTM, 21 Sept. 2012.
- [12] W-D. Zhang, P. H. Q. Pham, E. R. Brown, and P.J. Burke, "AC conductivity parameters of graphene derived from THz etalon transmittance," *Nanoscale* **6**, 13895-13899, 2014.
- [13] E.R. Brown, W-D. Zhang, L. Viveros, D. Neff, N.S. Green, M.L. Norton, P.H.Q. Pham, and P.J. Burke, "Sensing of DNA by graphene-on-silicon FET structures at DC and 101 GHz," *Sensing and Bio-Sensing Research*, pp. 19-23 (18 June 2015), <http://dx.doi.org/10.1016/j.sbsr.2015.05.002>.
- [14] Y-Y. Wang and P.J. Burke, "A large-area and contamination-free graphene transistor for liquid-gated sensing applications," *Appl. Phys. Lett.* **103**, 052103, 2013.
- [15] P. H. Bolivar, *et al.*, "Measurement of the dielectric constant and loss tangent of high dielectric constant materials at terahertz frequencies," *IEEE Trans. Micro. Theory and Tech.* **51**, 1062-1066, 2003.
- [16] K-F. Mak, M.Y. Sfeir, Y. Wu, C-H. Lui, J.A. Misewich, and T.F. Heinz, "Measurement of the optical conductivity of graphene," *Phys. Rev. Lett.* **101**, 196405, 7 November 2008.